EGG 1183-2373

EG&G

Energy Measurements Group

RECALIBRATION OF P-2 STANDARD IONIZATION CHAMBER

JUNE 1978

PREPARED FOR THE U.S. DEPARTMENT OF ENERGY
UNDER CONTRACT NO. EY-76-C-08-1183

SANTA BARBARA OPERATIONS
EG&G INC. 130 ROBIN HILL RD., GOLETA, CALIF. 93017

NOTICE

EG&G

Energy Measurements Group

EGG 1183-2373
S-666-R

RECALIBRATION OF P-2 STANDARD IONIZATION CHAMBER

by

J. Lewis Detch, Jr.

JUNE 1978

This report is unclassified: H. M. Borella
Classification Officer

Work performed for Los Alamos Scientific Laboratory through the Nevada Operations Office of the Department of Energy through Contract No. EY-76-C-08-1183

This page left blank intentionally.

ABSTRACT

Experimental and analytical techniques are described which permitted recalibration of the P-2 chamber's monoenergetic sensitivity based upon combined responses from a set of bremsstrahlung measurements, monoenergetic isotopic source measurements, and a monoenergetic gamma radiation produced by inelastic proton scattering. A novel technique is described for combining simultaneous knowledge of bremsstrahlung and monoenergetic response measurements with a statistically determined least structures constraint. The experimental details, analytical procedures, and resulting calibration of the standard P-2 ionization chamber from 100 keV to 20 MeV are presented and compared with previous determinations of the P-2 chamber sensitivity. Differences of approximately 15% between the derived sensitivity and the previously accepted values were observed in the region between 1.5 and 6 MeV.

ACKNOWLEDGEMENTS

Drs. John Pruitt and Steve Domen of the National Bureau of Standards are gratefully acknowledged for their encouragement, information, and helpful discussions relating to calibrations of this detector. Drs. Steve Caldwell, Darrell Drake, Peter Lyons, Joe Mack, and Carlton Young of the Los Alamos Scientific Laboratory contributed invaluably and assisted with the experimental measurements, especially those relating to the Van de Graaff accelerator facility at LASL, and provided Monte Carlo calculations of bremsstrahlung spectra. James Pigg, Helmar Janée, and Paul Zagarino contributed major efforts in data acquisition, reduction, and interpretation. Robert Elliott is thanked for his contributions and expertise in taming the computer. The contributions of Norman Voehl and the accelerator technicians to the reliable operation of the linear electron accelerator facility are gratefully acknowledged, as are the numerous suggestions and encouragements of Neil Norris and Lonnie Hocker who made essential contributions to the success of these experiments.

CONTENTS

ILLUSTRATIONS

ILLUSTRATIONS (continued)

TABLES

1. INTRODUCTION

This report covers work by the Detector Group at EG&G's Santa Barbara Operations (SBO) to recalibrate the standard P-2 ionization chamber, an air-filled aluminum alloy ionization chamber for use with radiation beam diameters up to 20 cm. It was designed and previously calibrated by Drs. Pruitt and Domen[1] of the National Bureau of Standards, and has been widely used as a secondary standard of radiation dosimetry. However, comparison of the P-2 chamber with a number of other detectors and a variety of radiation sources revealed a number of inconsistencies below 10 MeV.

Pruitt and Domen originally calibrated the P-2 chamber by accurately measuring its response to radiation relative to standardized calorimeters. They used filtered x-ray sources between 100 and 250 keV, isotopic sources of ^{137}Cs and ^{60}Co at 0.66 and 1.25 MeV, respectively, and thin-target bremsstrahlung produced with electron kinetic energies between 6 and 170 MeV. They then applied the Schiff[2] (thin-target) bremsstrahlung spectrum above 6 MeV to unfold a monoenergetic detector sensitivity which was smoothly joined to their monoenergetic measurements below 1.25 MeV.

In the course of calibrating a number of other radiation detectors[3] certain inconsistencies arose which suggested a discrepancy in the accepted monoenergetic sensitivity of the P-2 chamber in the energy region between 1.25 and 6 MeV. Our approach was to 1) measure the P-2 chamber's response to known bremsstrahlung spectra generated with electron energies between 0.5 and 20 MeV, 2) incorporate the monoenergetic and isotopic measurements of Pruitt and Domen, 3) apply a statistically determined constraint of least structures to the resulting monoenergetic sensitivity function, and 4) solve a set of Fredholm integral equations of the first kind, thus obtaining the monoenergetic sensitivity for the P-2 chamber. Our initial determination of this sensitivity was found to be in good agreement with that of Pruitt and Domen in the regions of overlapping experimental data. However, a discrepancy in the monoenergetic sensitivity of about 15% was initially observed near 3 MeV. To resolve this apparent discrepancy we measured the P-2 chamber's monoenergetic sensitivity with 4.4-MeV gamma rays which were produced by inelastic scattering of protons from ^{12}C. Within the

experimental errors (Section 5) this measurement of chamber response more closely agreed with our determination of the monoenergetic sensitivity at 4.4 MeV. We included this additional measurement in the unfold for the chamber's monoenergetic sensitivity. Our determination agrees essentially with the Pruitt and Domen measurements for energies below 1.25 MeV and between 8 and 20 MeV; however, our solution appears less oscillatory.

In addition to the detector's monoenergetic sensitivity, we also present our determinations of the instrument's response to thick-target bremsstrahlung continuum for electron kinetic energies between 0.5 and 20 MeV. Our data are in general agreement with the Pruitt and Domen measurements, whose lowest bremsstrahlung energy was 6 MeV. The small systematic differences between the two determinations are interpreted as being due to the use of slightly different bremsstrahlung spectra.

We present response measurements for the P-2 chamber to thick-target bremsstrahlung produced with electron kinetic energies between 0.5 and 20 MeV utilizing two collimation geometries and a comparison of these data with the calorimetric data of Pruitt and Domen. Our determination of the monoenergetic sensitivity of this detector is compared with Pruitt and Domen's determination, with monoenergetic measurements, and with our measurement at 4.4 MeV. Standard deviations in the solutions derived from experimental errors are presented.

2. EXPERIMENTAL METHOD

This section discusses the geometry of the radiation measurements, electronic equipment used for charge measurements, details of the radiation spectra and dosimetry, and various linac parameters. The detector's response to bremsstrahlung are determined from these measurements. The desired detector monoenergetic sensitivity is obtained from the solution of a set of simultaneous integral equations by a technique to be described in Section 3.

2.1 GEOMETRY

We employed two standardized collimation geometries, using tapered lead collimators of 1- and 2.5-inch-diam exit apertures, located 22.5 inches from the radiation source. These collimators were truncated right circular cones with the apex located at the radiation source, and represent variations from those normally used in routine isotopic source calibrations and bremsstrahlung radiation measurements. The experimental geometry for the bremsstrahlung measurement using the 1-inch-diam collimator is shown in Fig. 1. Except for the diameter of the collimator exit aperture and cone angle, the geometry for the 2.5-inch collimator was identical.

Previous linac response measurements[4] have shown that a tapered collimator is preferable to a straight wall collimator because: 1) the photon beam may be better defined since effects of the exit beam penumbra from the collimator may be reduced sufficiently to be neglected, 2) the production of secondary electrons from the collimator walls is minimized as small-angle scattering of photons from the collimator walls is minimized, and 3) we found that the tapered collimators effectively eliminated the 75-keV lead fluorescent x-ray present with other collimation geometries. Elimination of both the wall scatter from the collimators and of this particular fluorescent x-ray from the spectrum incident upon the detectors greatly facilitated the data analysis.

The tapered collimator design assumed a point radiation source, but in practice a true point source is not available from the linac. However, the source diameter was rather small (less than 1-cm diam) and sufficiently distant (22.5 inches or 57.2 cm) that the point source assumption was demonstrated to be valid.

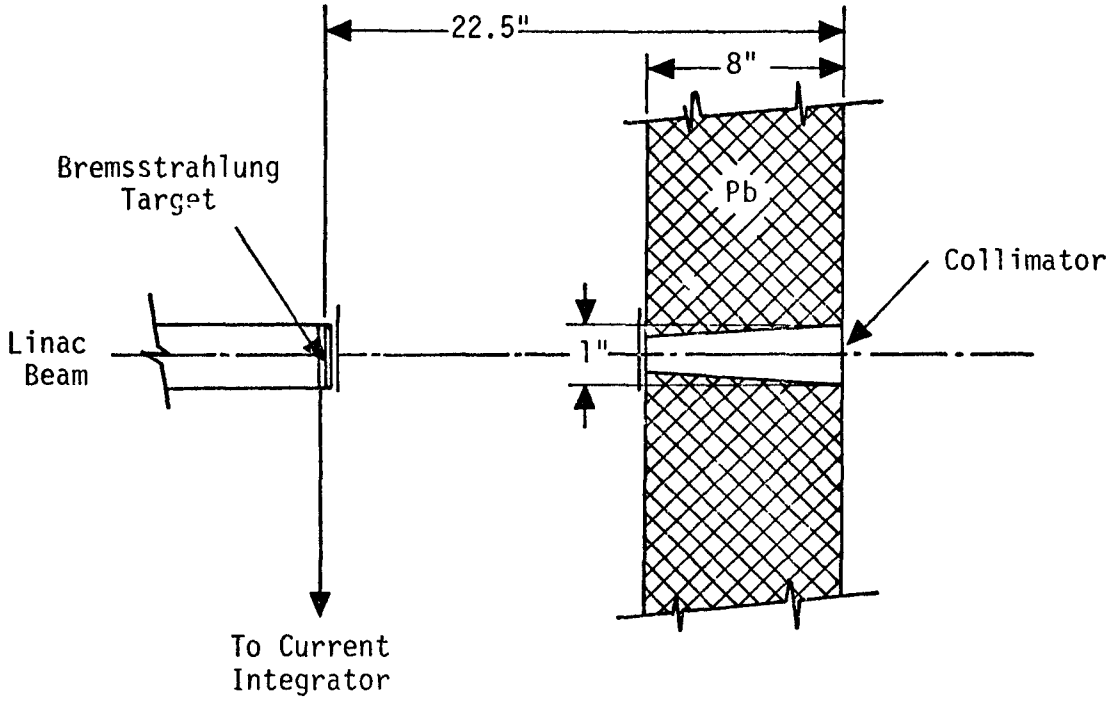

Fig. 1. One-inch-diam tapered collimation system

The detector was surrounded by an additional lead shield to reduce room-scattered radiation, and in particular to prevent irradiation of the detector from the sides and rear by the 0.511-MeV positron annihilation radiation present in the experimental area. The P-2 chamber was found to be considerably more sensitive to radiation from the sides than from the front. The measured detector response was due to radiation incident on the front of the chamber through the collimator aperture and was independent of the radiation levels present in the room.

The P-2 chamber was operated with and without the "doghouse" or annihilation shield for several tuning parameters of low, intermediate, and high electron energies. With the shield in place the ratio of P-2 chamber output current to the current incident on the bremsstrahlung target was demonstrated to be constant. This ratio varied significantly in the absence of the annihilation shield, particularly at the lower electron energies. Measurements of the current ratio indicated that the room-scattered radiation was a function of accelerator tuning parameters.

A test with a Ge(Li) detector in the same shielding configuration verified the absence of any line structure in the incident spectra. Thus, Ge(Li) detector measurements confirmed that the fluorescent lead x-ray, which was observed to be significant using straight wall collimators, was virtually eliminated by the use of the tapered collimator at the linac. Thus, for measurements made at the linac with the chosen geometry it was determined that corrections were not necessary for collimator penumbra, 75-keV lead fluorescent x-radiation, or the 0.511-MeV annihilation radiation.

2.2 ELECTRONICS

The electronic instruments employed for the various charge measurements are shown in Figs. 2a and b. Depending on current levels one or two measuring techniques was employed to measure the P-2 ionization chamber charge and electron beam charge incident on the bremsstrahlung target. For current levels greater than 10^{-12} A, an Ortec 439 current digitizer was employed with common timing used to gate the recording scalers on and off simultaneously, as illustrated in Fig. 2a. For detector currents less than 10^{-12} A, Cary Model 401 vibrating reed electrometers were located close to the detector and target to minimize radiation-induced current in the microdot low-noise signal cable. The vibrating reed assemblies were well shielded with 4 inches of lead in a structure having no straight path entry ports. The amplified signals from the Cary electrometer heads were cabled from the radiation cell in the existing cable trench. The Cary main electrometer chasses were maintained in low noise environments. High quality Victoreen electrometer resistors and nonpolarized polyethylene capacitors in an RC network were used to equalize the time constants of the two electrometers, whose outputs were recorded on a Houston Model 3000 dual pen plotter. To read the currents directly from the instruments it was necessary to equalize these time constants; otherwise, graphical integration of these currents would have been a time-consuming process. To average short term drift in the linac beam current these time constants were set to be quite long (100 sec). The electron stopping block was periodically inserted in the beam to obtain background or leakage current measurements (this technique produces the square wave signal traditionally used in calibrating detectors at isotopic source facilities). The ratios of the net detector and net bremsstrahlung target currents were thus measured directly from the strip chart paper. Several of these data sets were integrated with a planimeter to verify that the time constants had been properly

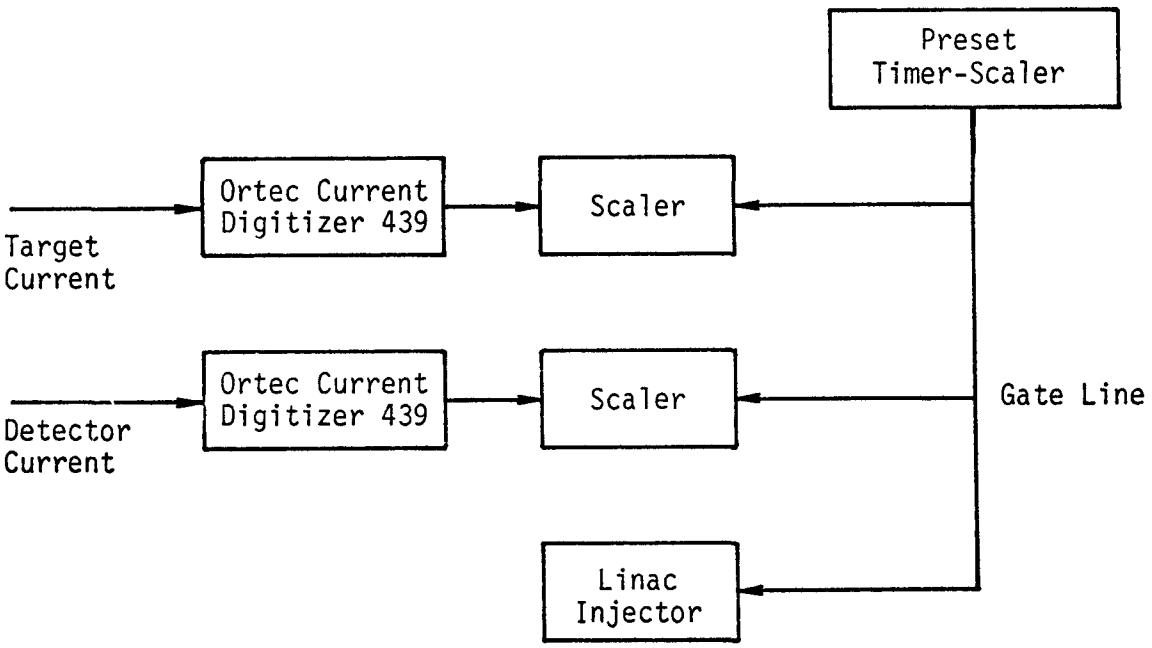

a. Current digitizer measurement system

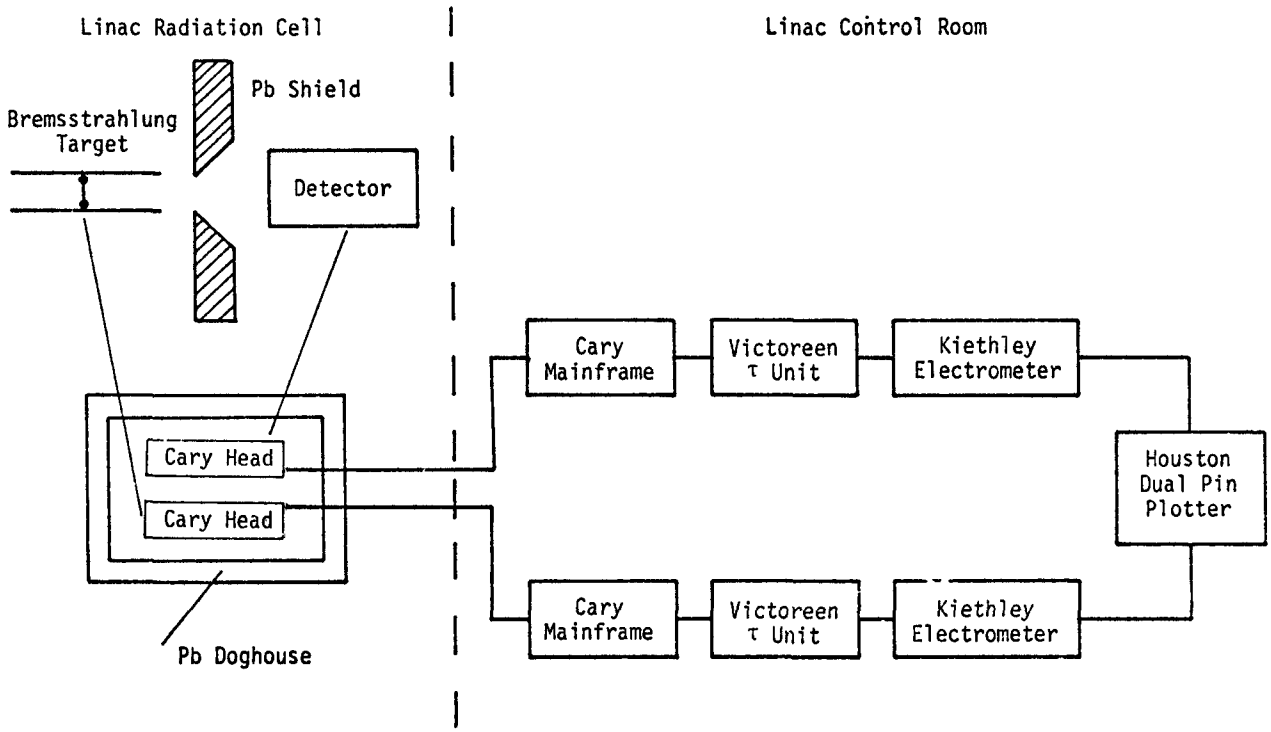

b. Cary electrometer block diagram

4694

Fig. 2. Charge measurement electronics

equalized, thereby justifying the direct reading of current at a common time. Due to occasional moderate drift in the electron beam intensity throughout the course of a detector measurement, several readings at various intervals of time and amplitude were averaged. When the current levels required changing between the current digitizers and current recorders, readings were taken with each system to confirm consistency in the data. These charge measurement systems were regularly calibrated with a Keithly Model 261 picoampere source whose calibration is NBS traceable. The Cary measurements system is illustrated in Fig. 2b.

2.3 BREMSSTRAHLUNG TARGET

The EG&G standard bremsstrahlung target, shown in Fig. 3, consists of 0.010-inch-thick tungsten backed by 0.005-inch-thick gold. The target was water cooled with a flow rate of three gallons per minute at 25 psi through an internal space in the target. Water thickness in the bremsstrahlung production areas of the target was 0.020 inch.

Electrons of energy less than approximately 14 MeV are absorbed in the attached 1.125-inch-thick aluminum stopping block. At higher electron energies, electrons penetrated the entire target assembly, and the collected charge was corrected for these losses. Correction factors for target penetration previously measured at SBO by R. Knowlen, C. Sandifer, and J. Pigg[5] were used in this work. An external sweeping magnet (not shown in Fig. 1) was included between the target and collimator to prevent electrons exiting the target from reaching the detector being studied.

At energies below approximately 5 MeV, primary electron backscatter from the target contributes significantly to charge measurement errors and was corrected by application of a Monte Carlo calculation by J. Mack.[6] An empirical parameterization of electron backscatter by Tabata, et al,[7] is in general agreement with the Monte Carlo calculations for our geometry done by Mack, but does not include effects of the substantial solid angle presented by the support structure for the tungsten-gold target. For computational purposes the radiation contributed by the 0.020-inch thickness of cooling water is neglected.

2.4 LINEAR ACCELERATOR OPERATION PROCEDURES

The electron energy was determined by use of 90° bending magnets whose magnetic field strength was accurately calibrated to within 0.5%. All electrons

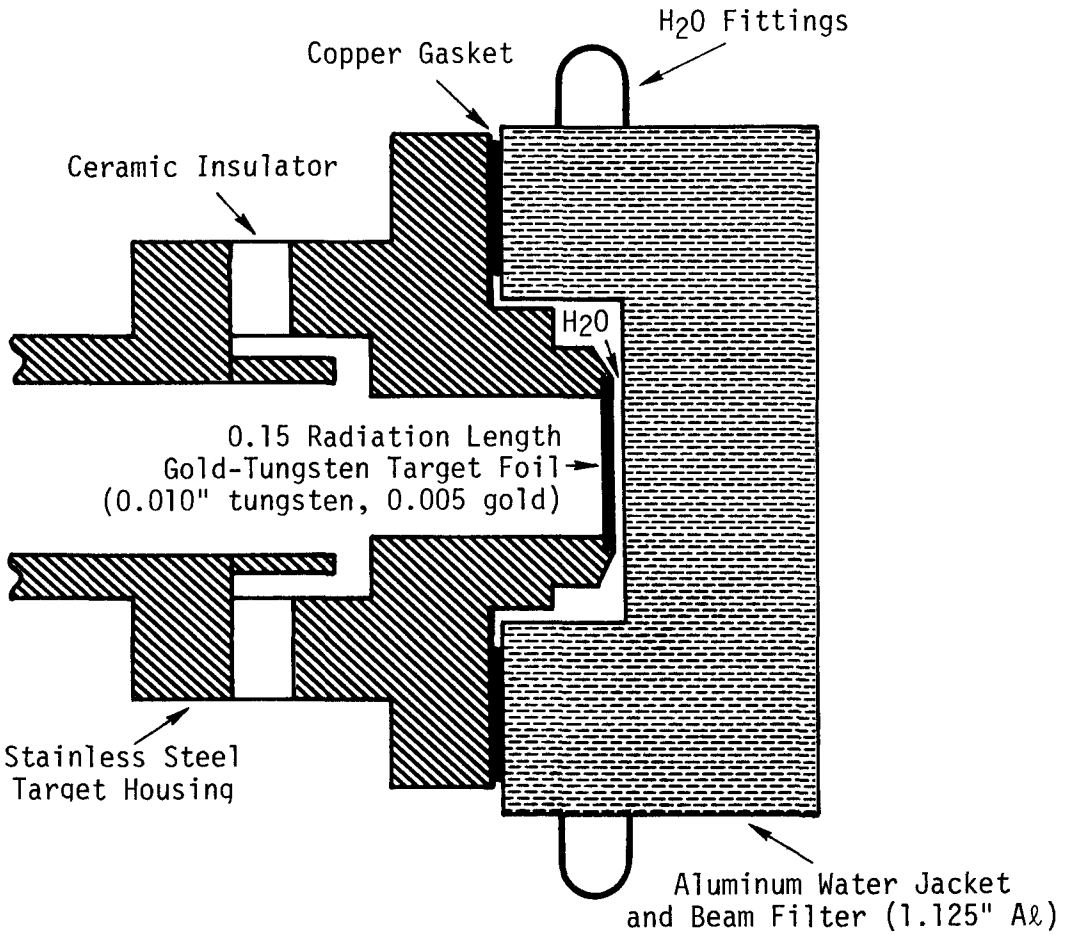

Fig. 3. Bremsstrahlung target used during linac calibration experiments

not within the acceptable energy limits, as determined by the bending radii of the magnets, were removed from the beam by adjustable mechanical slits. The magnetic field in the analyzing magnet was set to the desired electron energy, and the accelerator was tuned for optimum current and focal properties. Final energy measurements were made relative to a Bell Model 660 Digital Gaussmeter. The gaussmeter was properly warmed up in the radiation cell, and its Hall effect probes were then calibrated before and after setting the magnetic field of the bending magnets. This probe calibration was made with a ceramic magnet whose field strength value is NBS traceable. This calibration procedure minimizes errors caused by equipment instabilities, changes in line voltages, temperature changes, or amplifier gain changes. Uncertainty in the electron energy, possibly due to magnetic field dependent changes of the effective radius of curvature of

the electrons in the analyzing magnets, is believed to contribute no more than a few percent to the uncertainty in the absolute electron kinetic energy.

The uncertainty in kinetic energy due to a fractional uncertainty in the effective bending radius of the magnetic analyzer is approximately:

$$\Delta E \approx \frac{\left(\left(E + m_o c^2\right)^2 - \left(m_o c^2\right)^2\right)}{\left(E + m_o c^2\right)} d\rho/\rho \qquad (1)$$

where:

ΔE = uncertainty in electron kinetic energy

E = kinetic energy of the electron

$m_o c^2$ = rest mass energy of the electron

$d\rho/\rho$ = fractional uncertainty in the radius of curvature

The fractional error in the energy varies from about one and one half times that of the radius of curvature at electron kinetic energies of 0.511 MeV to 1.02 times that in the radius of curvature for an energy of 30 MeV.

The electron energy deviation, ΔE, determined by the slit width, was arrived at by requiring sufficient current on the target to produce an acceptable signal to noise ratio in the detector output signal. This ratio depends mainly on detector sensitivity and linac energy. At low energies the maximum available linac current decreases drastically, the bremsstrahlung production decreases with decreasing electron energy, and the detector sensitivity decreases below about 1 MeV. Thus it becomes necessary to open the energy analyzing slits to permit enough electrons to reach the target so that a usable detector signal may be obtained. Slit widths of 2% or less were maintained for energies above 1.5 MeV, and (with several minor exceptions) slit widths of 3% and 5% were used at 0.5-MeV electron energy.

This page left blank intentionally.

3. BREMSSTRAHLUNG SPECTRA

The thin-target (single interaction) bremsstrahlung production differential cross-section has been calculated by Bethe and Heitler.[8] This cross-section was subsequently integrated over electron recoil angles by Schiff[2] to produce a bremsstrahlung production cross-section which is differential in photon energy and solid angle. A number of significant assumptions are inherent within these basic derivations. The Bethe-Heitler derivation is based on application of the Born approximation, which requires that the atomic number of the target material be small in comparison with $137/(2\pi)$, which limits the proper validity to low-Z target materials. In addition, Schiff evoked an approximation which required that all energies be large in comparison with the electronic rest mass (0.511 MeV). Thus, Schiff's approximations properly limit the validity of the calculations to photons of energies greater than the electronic rest mass (to preserve "large" photon energies), but to photon energies less than the difference between the electron kinetic energy and the electronic rest mass (to preserve "large" recoil energies). In practice the Bethe-Heitler-Schiff[2,8] derivation produces good agreement with experiments over all photon energies of local interest and for thin, high-Z target materials. The slight differences between the Schiff bremsstrahlung cross-section and that produced by more rigorous derivations are negligible compared with the complexities introduced by the use of a thick-target. A number of other approximations for the calculation of bremsstrahlung are discussed by Koch and Motz[9] and elsewhere in the literature. Most of the more detailed treatments deal with the single interaction theory appropriate to thin target bremsstrahlung and include various correction terms to account for additional phenomena, such as coulomb wave effects, screening by the atomic electrons, etc.

The principal complications of thick target bremsstrahlung are energy loss mechanisms which rapidly decrease the electron kinetic energy and the multiple scattering processes which quickly change the angular distribution of the electrons, thus affecting the apparent angle (and cross-section) at which the bremsstrahlung photon is emitted.

The most rigorous thick target bremsstrahlung calculations have probably been performed by Berger[10] using Monte Carlo computational techniques with rather comprehensive bremsstrahlung production cross-sections and multiple scattering distributions. While these calculations are considered quite accurate the Monte Carlo calculation requires extensive computational expenditure to produce spectra with acceptable statistical errors.

Dickinson and Lent[11] performed a quasi-analytical calculation of thick target bremsstrahlung based on a technique by Hisdal[12] of conceptually subdividing a thick target into a number of thin laminae, calculating the contribution to the resulting radiation from each, and performing their sum attenuated by the appropriate mass attenuation coefficients to account for self attenuation in the remainder of the target. The Lent-Dickinson calculation assumes that the electron energy remains constant within an individual thin lamina, but that upon entering the subsequent target element the electron energy has been reduced by the appropriate range-energy relationship. We used this calculation with some success, though several hours of computational time on a CDC 7600 computer were required to produce spectra at the electron energies of interest with a rather coarse mesh of 21 photon energies. While the relative spectral shape appears to be in good agreement with experimental measurement, the calculated absolute intensity generally differs by a factor of about two from that actually observed or calculated by a technique to be described. The source of this discrepancy may be due to a programming error rather than a fundamental fault with the technique, and has not been further investigated.

Emigh[13] described a calculation of thick target bremsstrahlung which is based on an analytical integration of parameterized physical quantities combined with the Schiff bremsstrahlung production cross-section. Detch[14] extended Emigh's work to apply to a thick, multiple-component bremsstrahlung target and included effects of incident electron beam divergence, an improved approximation for multiple scattering within the target, and finite geometry corrections associated with the subsequent x-ray collimation. The Detch-Emigh calculation requires a few seconds of computational time to produce plausible bremsstrahlung spectra at a desired electron energy with a finer mesh of 80 photon energies.

A typical Detch-Emigh calculation is represented by the heavy solid line in Fig. 4, compared in absolute units with Mack's[6] Monte Carlo calculation and the O'Dell, et al,[15] absolute experimental measurements. The O'Dell, et al, measurements are represented by asterisks and are based upon the known[16] photodisintegration cross-section of the deuteron. The histogram with error bars was obtained by Mack using a Monte Carlo calculation derived from the work of

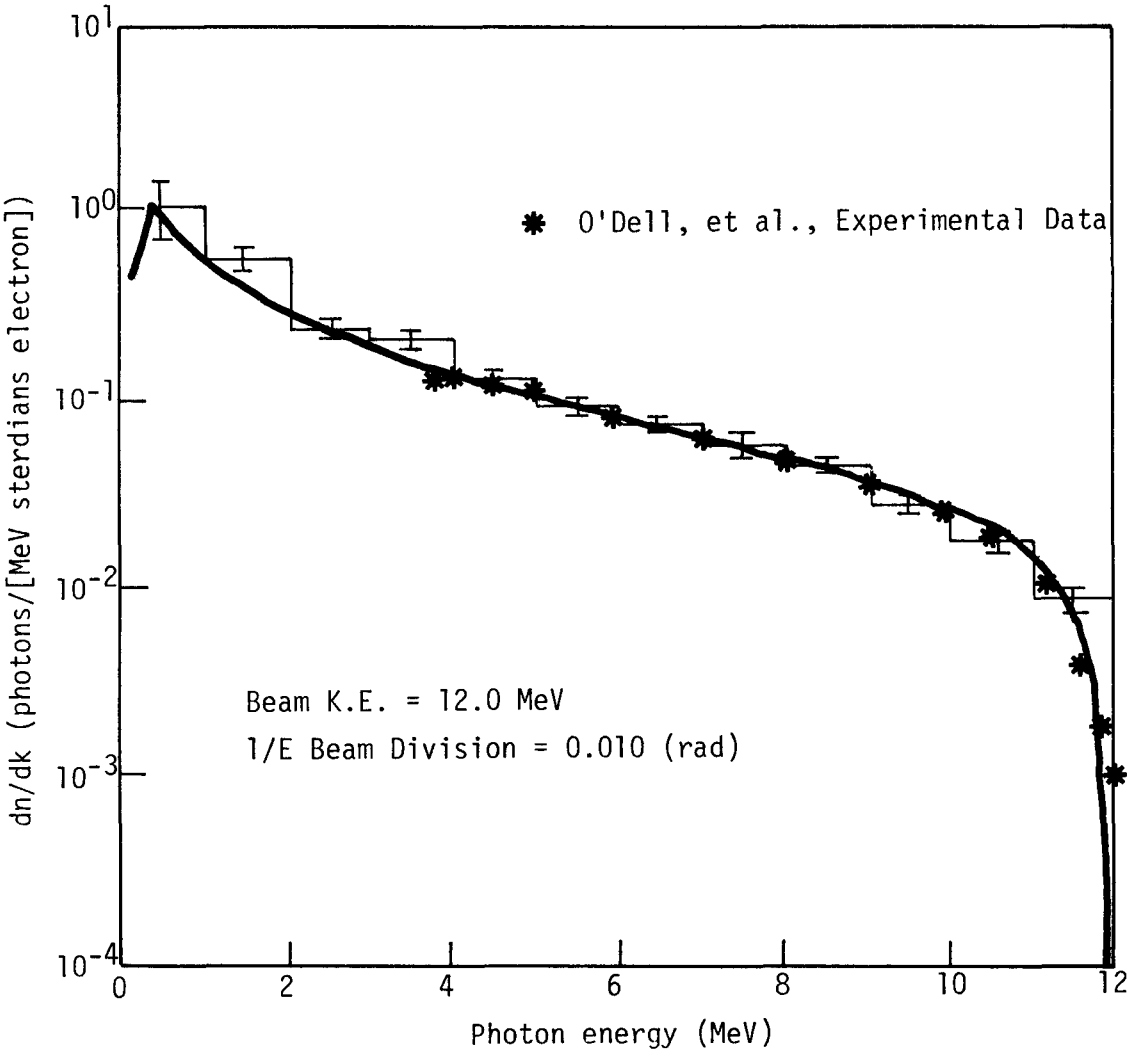

Fig. 4. Comparison of Detch-Emigh bremsstrahlung calculation with independent experimental and Monte Carlo data

Berger. Very good agreement may be seen among the experimental data, the Monte Carlo calculation, and the Detch-Emigh calculation used to generate bremsstrahlung spectra for the present series of experiments. The decrease in spectral intensity at the lowest photon energies is due to increased self-attenuation by the thick target.

For production of a photon having the electron's original kinetic energy the Schiff bremsstrahlung cross-section approaches zero, whereas Fano, Koch, and Motz[17] have shown that the bremsstrahlung cross-section is finite at the high energy limit. The minor discrepancy between the Detch-Emigh calculation and the

determinations of O'Dell, et al, and Mack at the high photon energy limit is interpreted as due to our use of the Schiff bremsstrahlung cross-section outside its limits of validity. The effects of this minor discrepancy on the unfolded monoenergetic detector response functions are negligible. We have limited the low-energy calculation to photon energies greater than 100 kV. The Detch-Emigh calculation appears to be in better agreement at low energies with experimental measurement and with more sophisticated calculations than would be expected from the numerous approximations employed in its derivation and application.

Figure 5 through 14 show the Detch-Emigh bremsstrahlung calculation at a variety of energies between 0.5 and 20.9 MeV, with comparison with either the Lent-Dickinson calculation for the standard target or with the photodisintegration data of O'Dell, et al, where available. The low-energy decrease in apparent bremsstrahlung production seen in the O'Dell data is due to an artifact in their data analysis caused by artifically forcing the count rate to be zero at the maximum observed time of their time-of-flight system before unfolding their data. The agreement with their absolute measurements of bremsstrahlung production of the standard target and the Detch-Emigh calculation is good. The previously used Lent-Dickinson calculation of the bremsstrahlung spectra may be seen to be consistently higher than either the Detch-Emigh calculation or the O'Dell, et al, data.

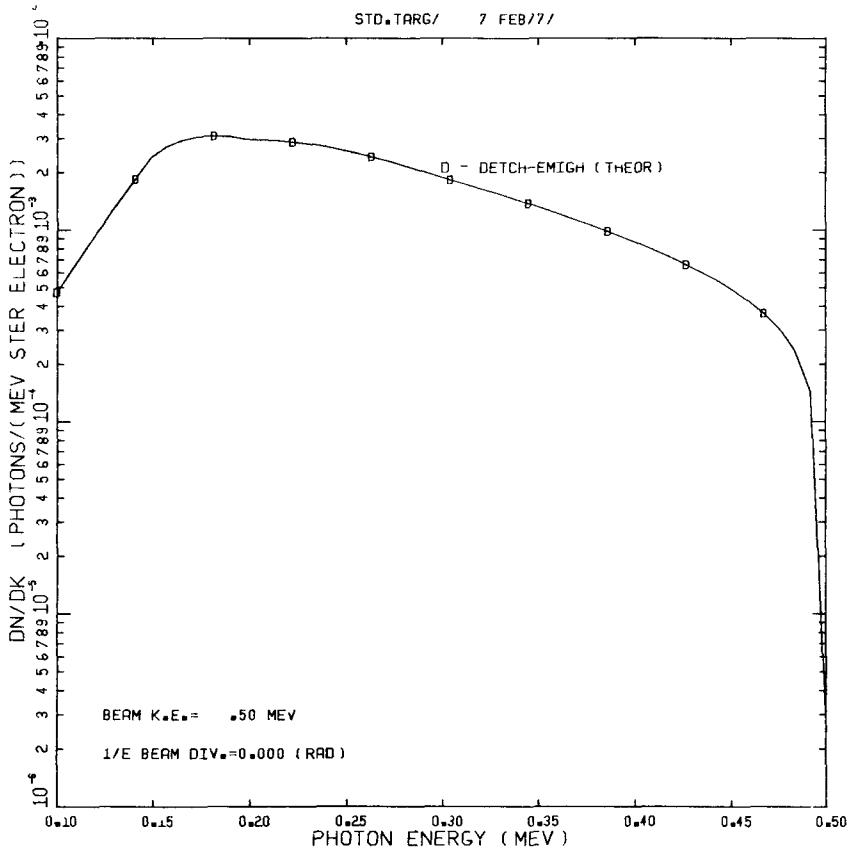

Fig. 5. Predicted bremsstrahlung spectrum at 0.5 MeV

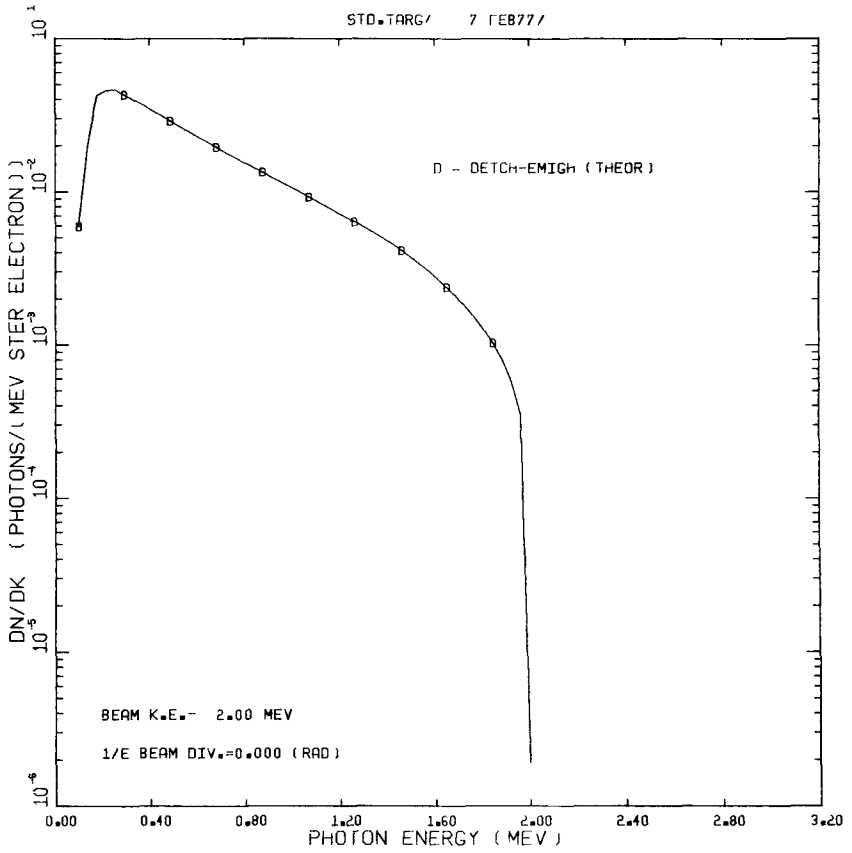

Fig. 6. Predicted bremsstrahlung spectrum at 2.0 MeV

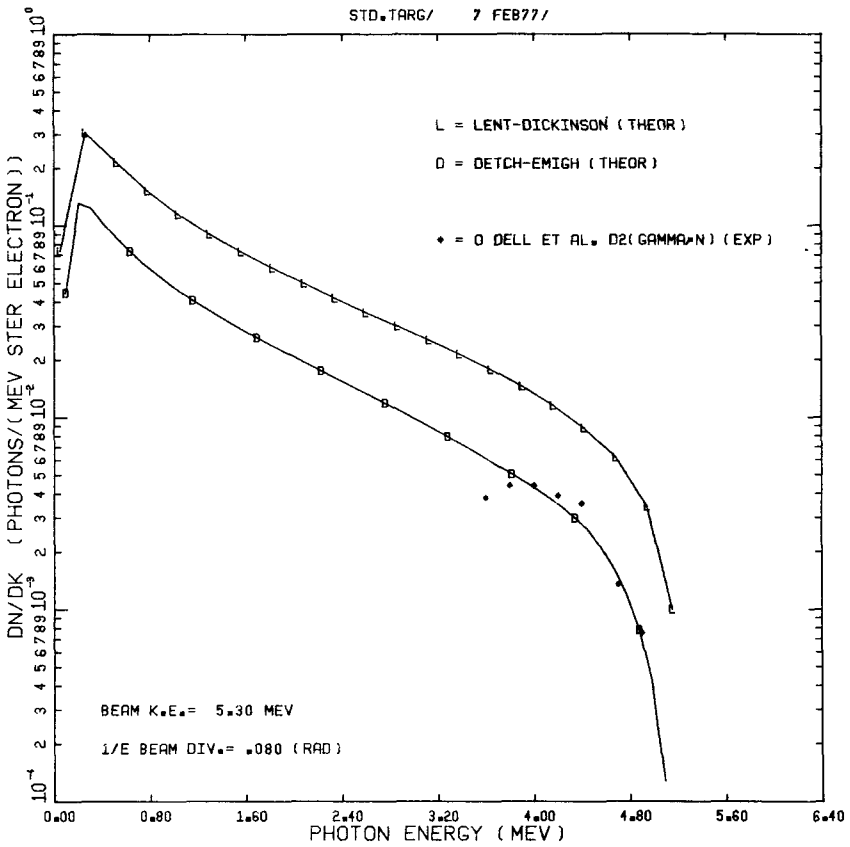

Fig. 7. Comparison of Detch-Emigh bremsstrahlung calculation with Lent-Dickinson calculation and O'Dell, et al, experimental measurements at 5.3 MeV

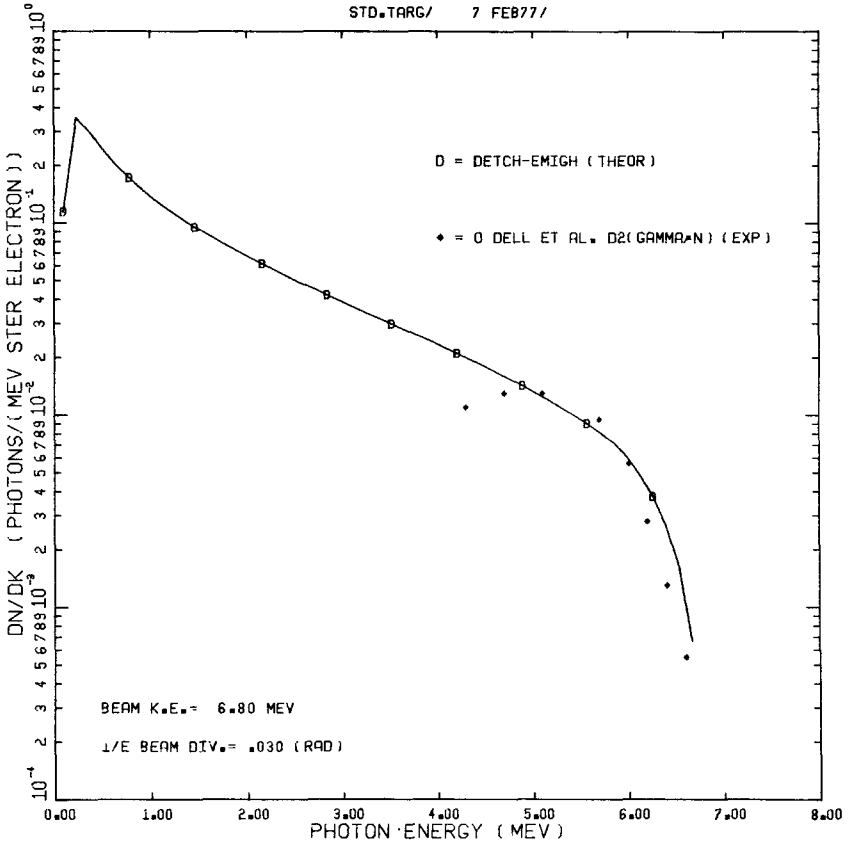

Fig. 8. Comparison of Detch-Emigh bremsstrahlung calculation with experimental measurements of O'Dell, et al, at 6.8 MeV

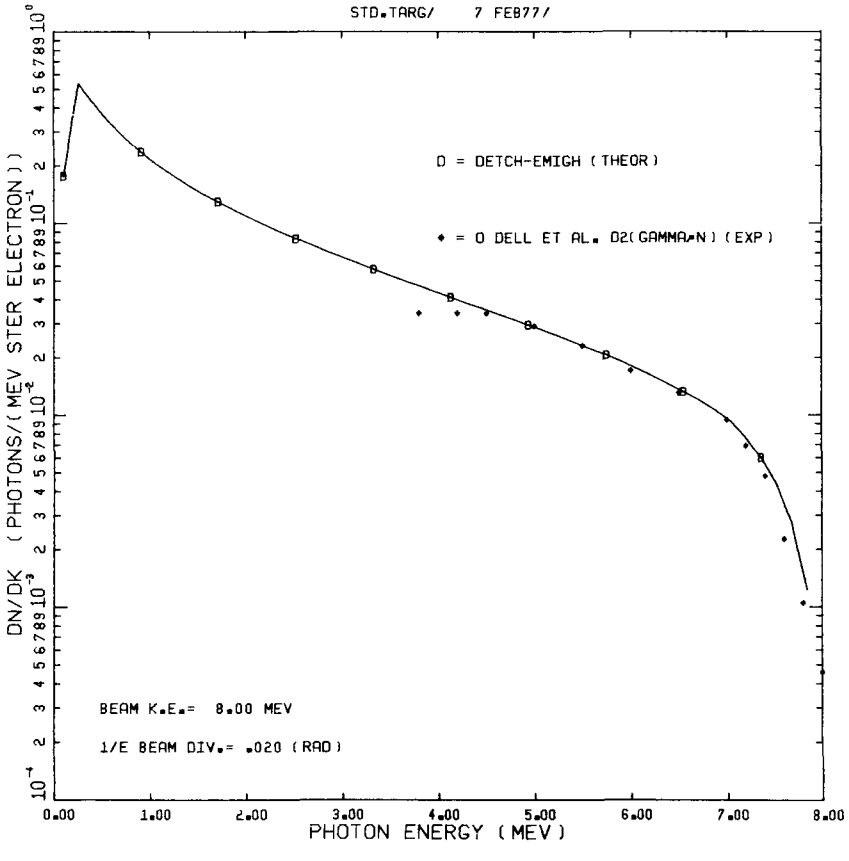

Fig. 9. Comparison of Detch-Emigh bremsstrahlung calculation with experimental data of O'Dell, et al, at 8.0 MeV

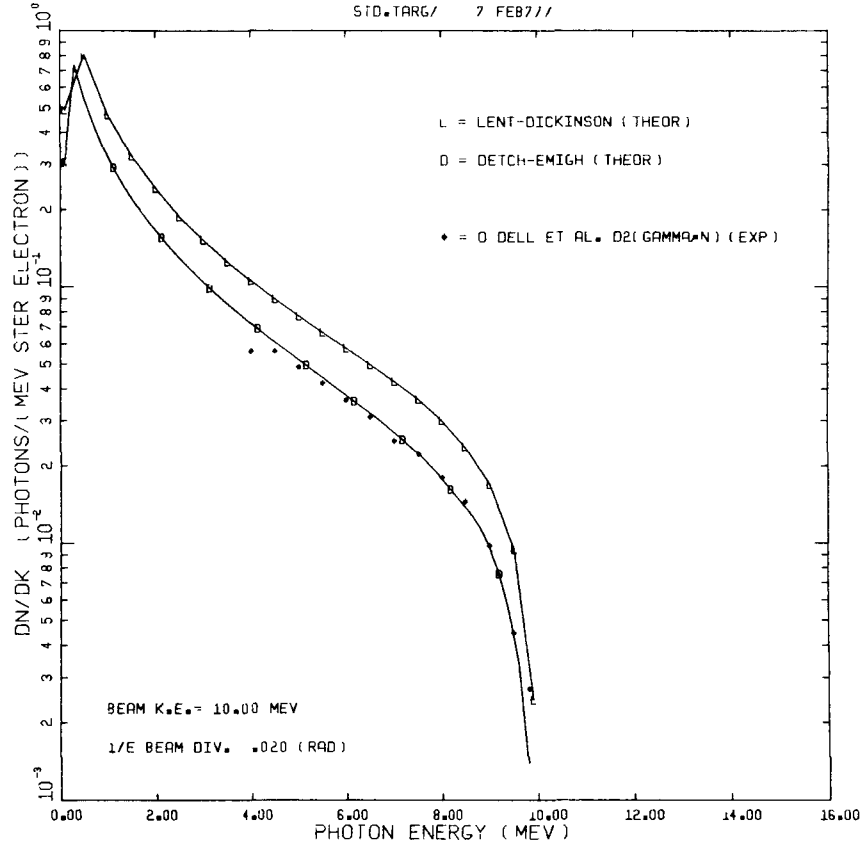

Fig. 10. Comparison of Detch-Emigh bremsstrahlung calculation with Lent-Dickinson calculation and experimental data of O'Dell, et al, at 10.0 MeV

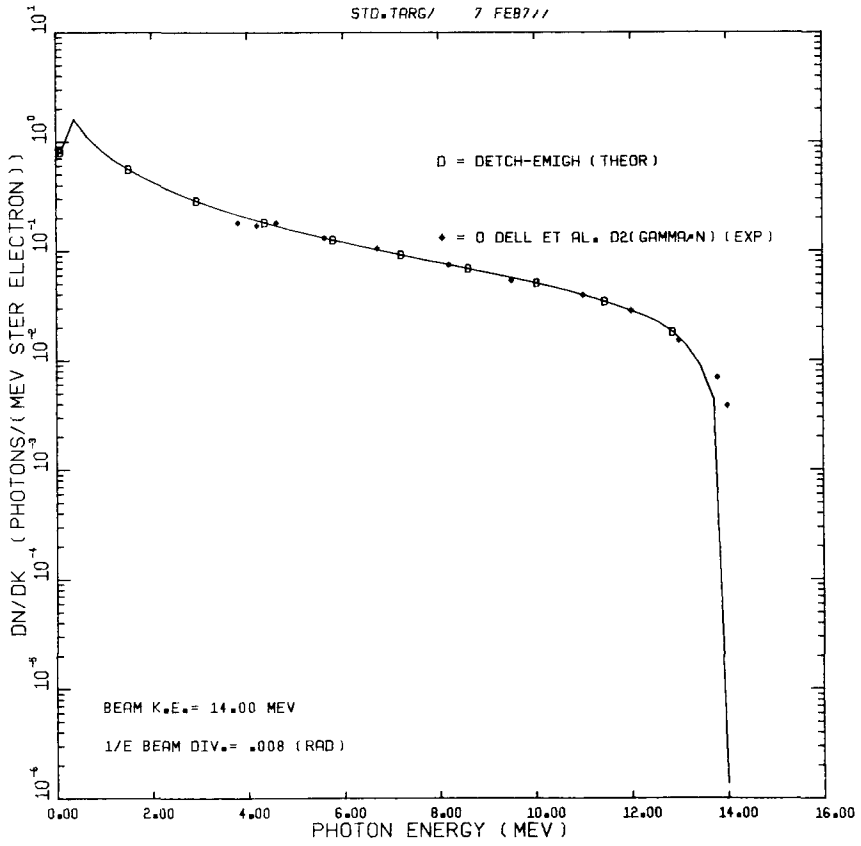

Fig. 11. Comparison of Detch-Emigh bremsstrahlung calculation with experimental measurements of O'Dell, et al, at 14.0 MeV

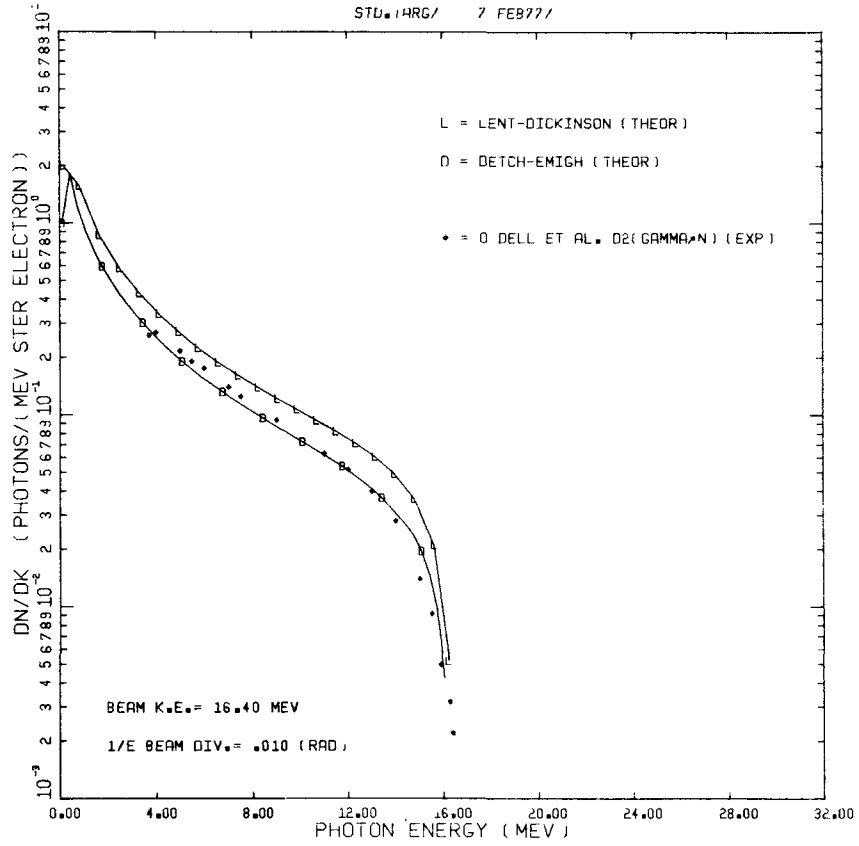

Fig. 12. Comparison of Detch-Emigh bremsstrahlung calculation with Lent-Dickinson calculation and experimental measurements of O'Dell, et al, at 16.4 MeV

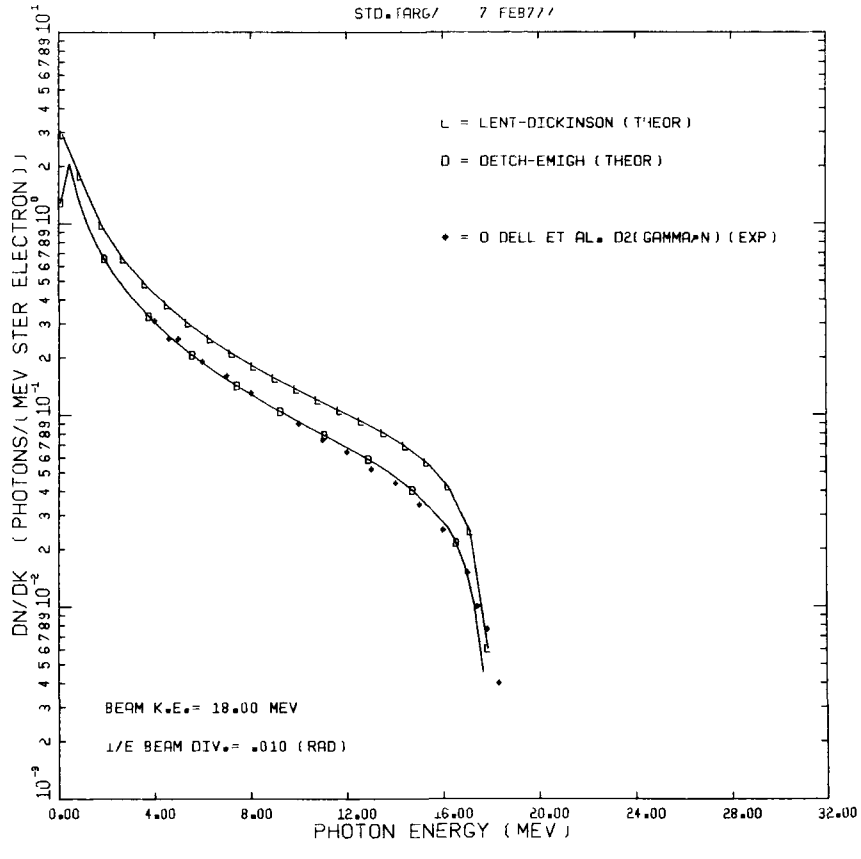

Fig. 13. Comparison of Detch-Emigh bremsstrahlung calculation with Lent-Dickinson calculation and experimental measurements of O'Dell, et al, at 18.0 MeV

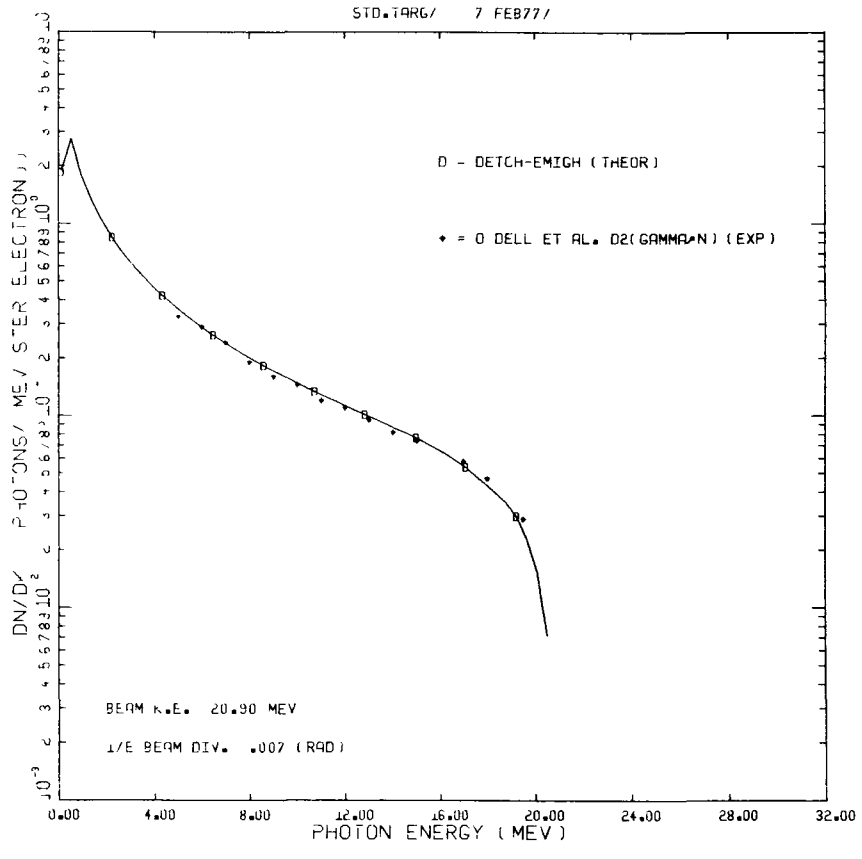

Fig. 14. Comparison of Detch-Emigh bremsstrahlung calculation with experimental measurements of O'Dell, et al, at 20.9 MeV

This page left blank intentionally.

4. UNFOLDING MONOENERGETIC RESPONSE FUNCTIONS - S(E)

4.1 INTRODUCTION

Three fundamental requirements that must be met to obtain monoenergetic detector sensitivities or response functions from a series of bremsstrahlung response measurements are: 1) one must accurately measure the detector response when irradiated with bremsstrahlung produced at a number of different electron energies, 2) one must know accurately the spectrum of the bremsstrahlung incident upon the detector, and 3) one must solve a set of Fredholm integral equations of the first kind to obtain the monoenergetic response function which appears as a factor of the integrand in the equations.

Measurement of detector response as a function of electron energy incident on the bremsstrahlung target has been addressed in the preceding sections. It should be noted that these response measurements may be performed relative to either of two standards. One may measure the detector response to the bremsstrahlung in a known geometry relative to the number of energetic electrons incident upon the target. This technique requires that one understand the effects of secondary, backscattered, and primary electrons which may otherwise escape from the target due to its finite dimensions. The number of incident electrons is usually obtained by measuring the electronic charge collected by a stopping target. An alternative method, which is dependent on reproducibility of the collimation geometry, requires comparison with a known standard detector appropriately normalized to an independent monitor or to the apparent charge collected on the bremsstrahlung target. Comparison with a standard detector requires very accurate knowledge of the bremsstrahlung spectrum and of the response of the standard detector to this particular spectrum. When properly performed both techniques demonstrate consistent results.

Knowledge of the bremsstrahlung spectrum produced by the target is subject to both experimental and theoretical uncertainties. We chose the approach of calculating the bremsstrahlung spectrum at the energies appropriate to the particular measurements, combined with experimental verification of the validity of the calculations at a few representative electron energies.

4.2 EXTRACTION OF MONOENERGETIC DETECTOR SENSITIVITY

If one had an intense variable energy source of monoenergetic gamma radiation, measurement of detector monoenergetic sensitivities would be straightforward. Conventional isotopic gamma sources of a few selected energies below about 2 MeV are available, and a few accelerator-produced reactions provide additional higher monoenergetic gamma energies. However, these sources do not provide the energy coverage necessary to determine a detector's monoenergetic sensitivity, and are rarely available with sufficiently intensity to permit calibration of detectors in the current output mode, being more suitable to counting experiments.

Bremsstrahlung radiation may be produced with sufficient intensity to operate detectors in the current output mode, and the end point or maximum photon energy produced may be varied within the limitations of the accelerator used to produce the radiation. However, bremsstrahlung is a continuum radiation, and the typical detector is sensitive over a fairly wide range of photon energies, so that the detector current output is proportional to the integral over energy of the product of the bremsstrahlung spectrum incident upon the detector multiplied by the detector monoenergetic sensitivity. This integral represents the detector's response to bremsstrahlung produced by a particular electron energy. By performing a number of detector response measurements to bremsstrahlung produced at a number of different electron energies, it is possible, in principle, to extract an equal number of monoenergetic sensitivities. However, in practice if this analysis is attempted by inverse matrix methods the kernel matrix is found to be nearly singular, which prevents reliable calculation of the inverse matrix.

We describe next a technique which avoids the matrix inversion problem by the use of a generalized linear system solver and the aid of a set of constraints representing a least structures requirement, which produces a plausible monoenergetic sensitivity consistent with the errors associated with the experimental measurements.

The charge produced by a radiation detector may be described by the following Fredholm equation of the first kind:

$$Q_d(E_i) = Q_{td}(E_i)\Omega \int_0^{E_i} B(E_i,E)\, S_d(E)\, dE \qquad (2)$$

where:

$Q_d(E_i)$ = charge produced by detector (coul)

$Q_{td}(E_i)$ = charge incident on target while detector is being irradiated (coul)

Ω = solid angle of x-ray collimation (sr)

$B(E_i,E)$ = differential bremsstrahlung production kernel (MeV/[MeV steradian coul])

$S_d(E)$ = desired detector monoenergetic sensitivity (coul/MeV)

E_i = electron energy incident on target (MeV)

E = bremsstrahlung photon energy (MeV)

The detector monoenergetic sensitivity, $S_d(E)$, represents the ratio of charge produced by the detector to the total energy present in the incident radiation. The detector monoenergetic sensitivity is also frequently expressed in units of (coul/joule), which is directly related by a multiplicative factor to the units used herein.

The total photon energy due to bremsstrahlung incident upon the detector may be represented by:

$$J_d(E_i) = Q_{td}(E_i)\Omega \int_0^{E_i} B(E_i,E)\, dE \quad \text{(MeV)} \tag{3}$$

The detector bremsstrahlung response may be expressed as the ratio of Eq. (2) to Eq. (3), representing the ratio of charge produced in the detector to the total energy incident upon the detector:

$$R_d(E_i) = Q_d(E_i)/J_d(E_i) \tag{4}$$

Note that the ratio in Eq. (4) is not explicitly dependent upon either the quantity of charge incident upon the target, $Q_{td}(E_i)$, or the solid angle defined by the collimation geometry if the measurements of $Q_d(E_i)$ and $J_d(E_i)$ are performed simultaneously, but it is dependent upon both if measured independently. Practical considerations usually necessitate separate measurement of these two quantities suitably normalized to an independent monitor or to the charge incident upon the target.

For convenience the bremsstrahlung kernel may be normalized to its own integral over photon energy:

$$B_n(E_i,E) = \frac{B(E_i,E)}{\int_0^{E_i} B(E_i,E)\, dE} \quad (MeV^{-1}) \tag{5}$$

The normalization of Eq. (5) permits the preceding equations to be expressed as:

$$R_d(E_i) = Q_d(E_i)/J_d(E_i) = \frac{\int_0^{E_i} B(E_i,E)\, S_d(E)\, dE}{\int_0^{E_i} B(E_i,E)\, dE} \quad , \text{ or} \tag{6}$$

$$R_d(E_i) = \int_0^{E_i} B_n(E_i,E)\, S_d(E)\, dE \quad (coul/MeV)$$

With a standard radiation detector with a known monoenergetic sensitivity, $S_d(E)$, and an understanding of the bremsstrahlung kernel produced by the particular target in use, one may calculate for this standard detector a bremsstrahlung response function, $R_s(E_i)$. For the detector in question, $R_d(E_i)$ may then be measured relative to the standard detector's response suitably normalized to an appropriate monitor or to the apparent target charge, if it can be demonstrated that the charge collected from both detectors is proportional to the apparent charge collected on the target. A preferable means of measuring the photon energy incident upon the detector would be through the use of a calibrated totally stopping calorimeter, which would largely avoid the uncertainties associated with either incomplete target charge collection or with the probable errors associated with the use of a standard detector whose response is known only approximately. However, a suitable calorimetor was not readily available.

Response functions for the detector at a variety of electron energies may be expressed directly in the form of Eq. (6) if the measurements are made relative

to a known standard detector. If the errors introduced by uncertainties in the solid angle subtended by the x-ray collimation geometry and the target charge measurement accuracy are comparable to the uncertainties associated with a measurement relative to a standard detector, one may rewrite Eq. (2) in the form:

$$R_d(E_i) = \frac{Q_d(E_i)}{Q_{td}(E_i)\Omega \int_0^{E_i} B(E_i,E)\, dE} = \int_0^{E_i} B_n(E_i,E)\, S_d(E)\, dE \quad \text{(coul/MeV)} \tag{7}$$

Having obtained a set of bremsstrahlung response measurements for the detector in the form of Eqs. (6) or (7), the integral in these equations may be approximated by the summation:

$$R_d(E_i) \approx \sum_j B_n(E_i,E_j)\, S_d(E_j)\, \Delta E_j \tag{8}$$

Retaining only the subscripts identifying the energies, Eq. (8) may be rewritten as matrix elements:

$$R_d(i) = \sum_j A_{ij}\, S_d(j) \tag{9}$$

where

$$A_{ij} = B_n(i,j)\, \Delta E_j \tag{10}$$

When expressed in this form, the use of a nonconstant photon energy interval, ΔE_j, may be allowed. In matrix notation Eq. (9) may be represented as the product:

$$\underline{R}_d = \underline{A}\, \underline{S}_d \tag{11}$$

A very versatile and powerful computing subroutine known as GLSS* (General

*GLSS is based upon techniques described in References 18, 19, and 20.

Linear System Solver) was obtained from the LASL Program Library to solve a modification of Eq. (11) to obtain the desired monoenergetic photon response function, $S_d(E_j)$, which appears as a column vector in the matrix equation. The bremsstrahlung kernel matrix defined in Eq. (10) was modified and appended to permit simultaneous solution for the monoenergetic response function, $S_d(E_j)$, using 1) bremsstrahlung measurements performed with different collimation geometries, 2) independent monoenergetic (gamma-ray) measurements, and 3) a statistically weighted least-structures constraint.

If we assume that there were (n) measurements of bremsstrahlung responses, then the first (n) rows of the $\underline{A}$ and $\underline{R}$ (Eq. 11) matrices contain the appropriate bremsstrahlung kernel elements and the response measurements. This technique permits multiple entries at the same electron energy with no restraint placed on the particular electron energy used to produce the measurement other than knowledge of the energy. To include independent measurements of the detector's monoenergetic response to gamma radiation, one attempts to force the appropriate element of the $\underline{S}_d$ column vector to reflect the independently measured value. The monoenergetic measurements are included by zero-filling the (n+1) row of the $\underline{A}$ matrix with the exception of the elements corresponding to the appropriate monoenergetic energy, which may be set equal to unity. In the event that the detector was irradiated with other than a monoenergetic radiation, the elements of the (n+1)-th row of the $\underline{A}$ matrix may be appropriately modified to reflect additional components in the irradiated spectrum. The (n+1)-th element of the response vector, $\underline{R}$, contains the response for the particular measurement. Thus, if there were both (n) bremsstrahlung measurements and (k) monoenergetic measurements, then the latter would occupy the (n+1)-th through the (n+k)-th rows of the $\underline{A}$ matrix and the $\underline{R}$ response vector. Appropriate weighting factors may be included on both sides of the matrix equation (in $\underline{A}$ and $\underline{R}$) to reflect the relative importance of the various measurements based upon their experimental errors.

The solution by inverse matrices would require choosing (n+k) different photon energies so that the $\underline{A}$ matrix becomes a square matrix, thereby obtaining the inverse of the A matrix by conventional means, and the desired monoenergetic sensitivity in the form:

$$\underline{S} = \underline{A}^{-1}\ \underline{A}\ \underline{S} = \underline{A}^{-1}\ \underline{R} \qquad (12)$$

The difficulty with the inverse matrix technique in this case is that the $\underline{A}$ matrix

is nearly singular, even after averaging or combining multiple measurements made at the same electron energy. A previous program was abandoned for this application when it was discovered that the product of its inverse matrix multiplied by the kernel matrix failed to produce the identity matrix due to accumulated computational truncation errors. This requirement of the inverse matrix is expressed as:

$$\underline{A}^{-1}\,\underline{A} = \underline{I} \tag{13}$$

One frequently desires to know the detector monoenergetic response function at a greater number of photon energies than there were bremsstrahlung measurements, a problem which is inherently underdetermined. When the subroutine GLSS is asked to solve an underdetermined solution it produces an exact, but physically unreasonable, solution for the detector monoenergetic response function. As an example, if one used 80 different photon energies in the $\underline{S}$ vector, which is also the number of columns in the $\underline{A}$ matrix, with a total of 20 bremsstrahlung and monoenergetic response measurements, the resulting exact solution for $\underline{S}$ produced by GLSS would consist of 20 nonzero values for $\underline{S}$ which would exactly satisfy Eq. (11). However, the distribution consisting essentially of a distribution of 20 delta functions in energy, with implied zero sensitivity at intermediate energies, is an unphysical and therefore unacceptable solution.

In the same manner that the monoenergetic experimental measurements were appended to the $\underline{A}$ or kernel matrix, a least structures constraint in the sense of minimized second numerical differences may be added to the $\underline{A}$ matrix. For an arbitrary function, $Y(x)$, the curvature of the function is proportional to the second derivative with respect to x, and the second derivative is approximately equal to the second numerical difference:

$$\left.\frac{\Delta^2 Y}{\Delta x^2}\right|_{x=x_i} \approx \frac{Y_{i+1} - 2Y_i + Y_{i-1}}{\Delta x^2} \tag{14}$$

Thus, a constraint that the function Y have no curvature ($d^2Y/dx^2 = 0$) in the vicinity of $x=x_i$ may be expressed in the matrix form:

$$\lambda \underline{G}\,\underline{Y} = 0 \tag{15}$$

where the elements of $\underline{G}$ are given by:

$$G_{ij} = \begin{cases} 1 & j = i \pm 1 \\ -2 & j = i \\ 0 & j \neq i \text{ or } j \neq i \pm 1 \end{cases} \tag{16}$$

The multiplicative constant, λ, appears essentially as a Lagrange multiplier.

If we chose (m) elements in the $\underline{S}$ vector, representing the monoenergetic sensitivity function at (m) different photon energies, then we may append (m-2) additional rows to the $\underline{A}$ and $\underline{R}$ matrices representing an attempted constraint towards least structures. The resulting (n+k+m-2) by (m) matrix forming $\underline{A}$ is overdetermined, and the subroutine GLSS produces in this case a solution which is the "best" fit in the sense of least square differences to all of the conflicting information contained in the $\underline{A}$ matrix.

Thus the form of the matrix Eq. (11) is represented as:

$$\begin{array}{r} \text{Bremsstrahlung Measurements Portion} \\ \\ \\ \\ \\ \text{Monoenergetic Measurements Portion} \\ \\ \text{Least Structures Portion} \\ \\ \\ \\ \\ \end{array} \left\{ \begin{array}{|cccccccc|} A_{11} & A_{12} & A_{13} & \cdot & \cdot & \cdot & \cdot & \cdot \\ A_{21} & A_{22} & A_{23} & \cdot & \cdot & \cdot & \cdot & \cdot \\ A_{31} & A_{32} & A_{33} & \cdot & \cdot & \cdot & \cdot & \cdot \\ \cdot & \cdot & \cdot & \cdot & \cdot & \cdot & \cdot & \cdot \\ A_{n1} & A_{n2} & A_{n3} & \cdot & \cdot & \cdot & \cdot & \cdot \\ \hline 0 & 0 & 0 & 1 & 0 & 0 & 0 & \cdot \\ 0 & 0 & 1 & 0 & 0 & 0 & 0 & \cdot \\ \hline \lambda & -2\lambda & \lambda & 0 & 0 & 0 & \cdot & \cdot \\ 0 & \lambda & -2\lambda & \lambda & 0 & 0 & 0 & \cdot \\ 0 & 0 & \lambda & -2\lambda & \lambda & 0 & 0 & 0 \\ \cdot & \cdot & \cdot & \cdot & \cdot & \cdot & \cdot & \cdot \\ \cdot & \cdot & \cdot & \cdot & \cdot & \cdot & \cdot & \cdot \\ 0 & 0 & 0 & 0 & \cdot & \lambda & -2\lambda & \lambda \end{array} \right| \left| \begin{array}{c} S_1 \\ S_2 \\ S_3 \\ S_4 \\ S_5 \\ \cdot \\ \cdot \end{array} \right| = \left| \begin{array}{c} R_1 \\ R_2 \\ R_3 \\ \cdot \\ R_n \\ \hline S_4' \\ S_3' \\ \hline 0 \\ 0 \\ 0 \\ 0 \\ 0 \\ 0 \end{array} \right| \tag{17}$$

The smoothness parameter, λ, is arbitrary at this point. If λ is set equal to zero the solution reverts to the physically unreasonable exact solution previously described. If λ is made too large the solution reverts to a linear function for S(E), being dominated by the requirement that the solution have

minimum numerical second differences, which may also be physically implausible. In the case that the smoothness parameter, λ, is too large the derived monoenergetic sensitivity function, S(E), is very smooth, but the differences between the implied response measurement (the refold) using the previous bremsstrahlung kernel and derived monoenergetic sensitivity and the actual measurements of bremsstrahlung response may be entirely unacceptable.

The choice of smoothness parameter may be made objectively based on errors in the original experimental data. The normalized Chi-squared deviations between the experimental data and the refold may be used to define a value of the smoothness parameter, λ. The refold produced by the matrix product of the smoothed S(E), and the bremsstrahlung kernel (the A matrix including only bremsstrahlung and monoenergetic portions) should be approximately equal to unity within 2%. In this manner one obtains the smoothest possible solution in the sense of minimized numerical differences consistent with the experimental errors in the original data. Further, the subroutine GLSS provides the variance and covariance matrices for the solution, so that the standard deviations of the obtained solution and the refold are present, based on the probable errors which are introduced through the weighting of the individual rows of the A matrix.

Thus, the refold of the bremsstrahlung kernel with the calculated monoenergetic sensitivity is represented by the integral:

$$R_{calc}(E_i,\lambda) = \int_0^{E_i} B(E_i,E)\, S(E,\lambda)\, dE \qquad (18)$$

In this manner the Chi-squared deviation between calculated and measured bremsstrahlung responses is a function of λ. By requiring that Chi-squared be equal to unity (within 2%), an objective means of applying the smoothness parameter was obtained. This particular answer is the smoothest solution for the monoenergetic sensitivity that is consistent with the statistical errors of the experiment.

This page left blank intentionally.

5. DATA PRESENTATION

A number of P-2 ionization chambers have been constructed according to an NBS design[1] and are widely used as secondary standards of dosimetry. At least eleven of these instruments used at accelerator facilities throughout the world have been calibrated against the NBS P2-4 chamber and were found to agree within a few tenths of one percent. The P2-4 chamber was calibrated relative to calorimeters by NBS for thin-target bremsstrahlung produced by electron kinetic energies between 6 and 180 MeV and beam intensities from 0.5 to 10^3 W/cm^2. Correction factors for air temperature, pressure, beam filtration, beam diameter, and variation in construction permit adjustment of the calibration factor of an arbitrary P-2 chamber to that of the original NBS unit. However, differences in bremsstrahlung spectral shape between that produced by thin and thick targets may introduce certain differences in apparent sensitivity for the P-2 chamber.

Two sets of experimental bremsstrahlung response measurements are presented in Fig. 15. The upper data set (asterisks with error bars) was taken using the 2.5-inch-diam exit aperture, tapered lead collimator located 22.5 inches from the thick standard bremsstrahlung target, with the P-2 chamber located immediately behind the aperture. The lower data set employed a similar 1-inch-diam tapered collimator with otherwise identical geometry. Both data sets presented in Fig. 15 represent experimental measurements of ratios of collected P-2 chamber charge to bremsstrahlung target charge corrected for experimentally measured non-total beam stoppage in the target. The dashed lines represent the calculated refolds of the derived P-2 chamber monoenergetic sensitivity with the Detch-Emigh bremsstrahlung kernel. When compared with the experimental measurements the calculated responses demonstrated a weighted Chi-squared distribution of unity (±2%).

Figure 16 represents the conversion of the Fig. 15 data to calorimetric units based upon the assumed validity of the Detch-Emigh bremsstrahlung kernel. Both sets of data (asterisks with error bars) demonstrate independence of the collimation geometry. The double dashed lines (not resolved in Fig. 15) represent standard deviations in the calculated refold as determined by experimental error. In Fig. 16 the letters "N" represent for comparison the NBS

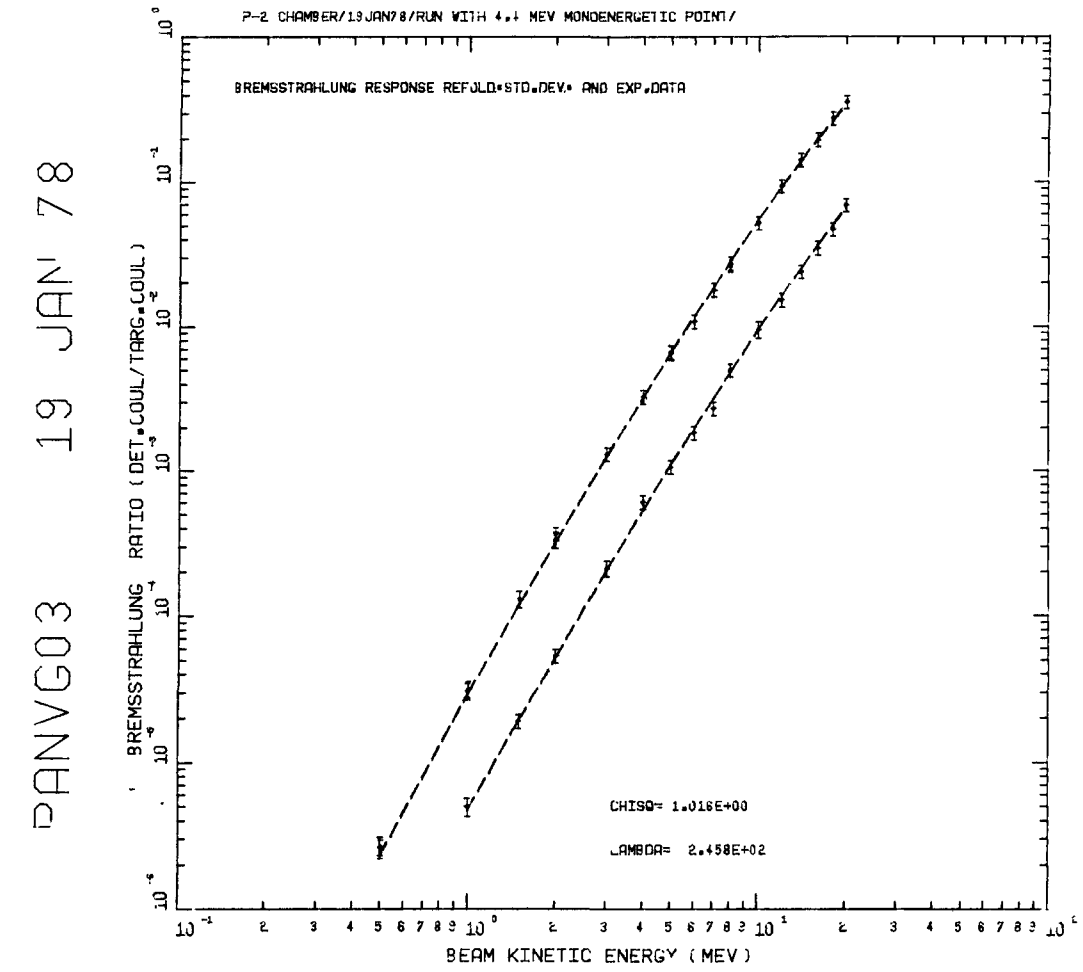

Fig. 15. Experimental charge ratio measurements and comparison with calculated refold for P-2 chamber

calorimetric measurements reported by Pruitt and Domen[1] for the P-2 chamber when irradiated with thin-target bremsstrahlung. Additional measurements of the P-2 chamber response to thin-target bremsstrahlung have been performed by Tomimasu, et al,[21] measured relative to a quantameter and are in general agreement with the NBS measurements. Due to differences in bremsstrahlung targets and subsequent x-ray filtration, the data presented in Fig. 16 are considered to be in good agreement above 6 MeV, the lowest energy measured by Pruitt and Domen.

Figure 17 compares the monoenergetic detector sensitivity for the P-2 chamber obtained by this analysis technique (described in Section 3) with that obtained by Pruitt and Domen. The asterisks with error bars represent their monoenergetic measurements made with filtered x-ray and isotopic sources, and

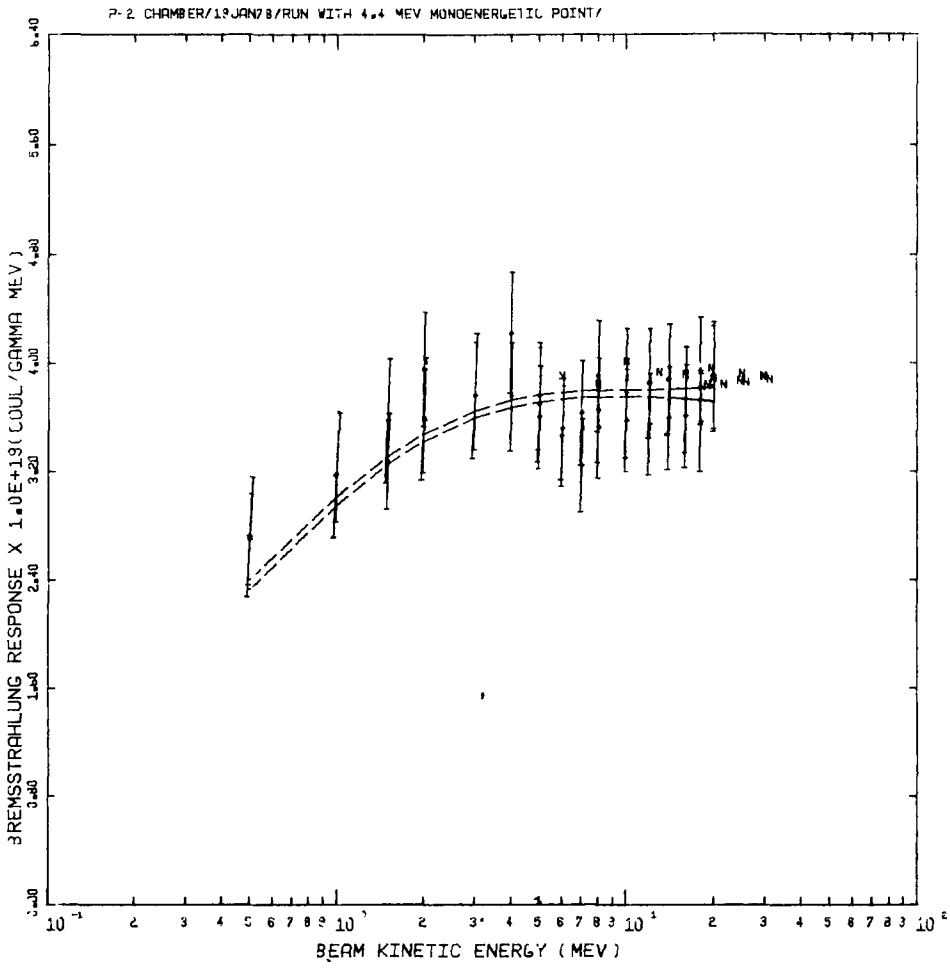

Fig. 16. Experimental data expressed in calorimetric units compared with calculated refold for P-2 chamber

the letters "N" represent their calculated values for the P-2 chamber monoenergetic sensitivity with data only for energies above 6 MeV. The connected plus signs with standard deviation envelope represent EG&G's calculated sensitivity function based upon the data shown in Fig. 15 and Pruitt and Domen's monoenergetic measurements. These calculations are in essential agreement in the regions where common data exist, specifically below 1.25 MeV and above 6 MeV. Drs. Pruitt and Domen[22] indicated that their calculations were subject to uncertainties in the region between 1.25 and 6 MeV, where our determinations differ by as much as 20%. Furthermore, the sensitivity function for the P-2 chamber which we obtained (the connected plus signs) was found to be the preferable calibration for producing consistency between monoenergetic sensitivities of other detectors unfolded from combined bremsstrahlung and isotopic measurements.

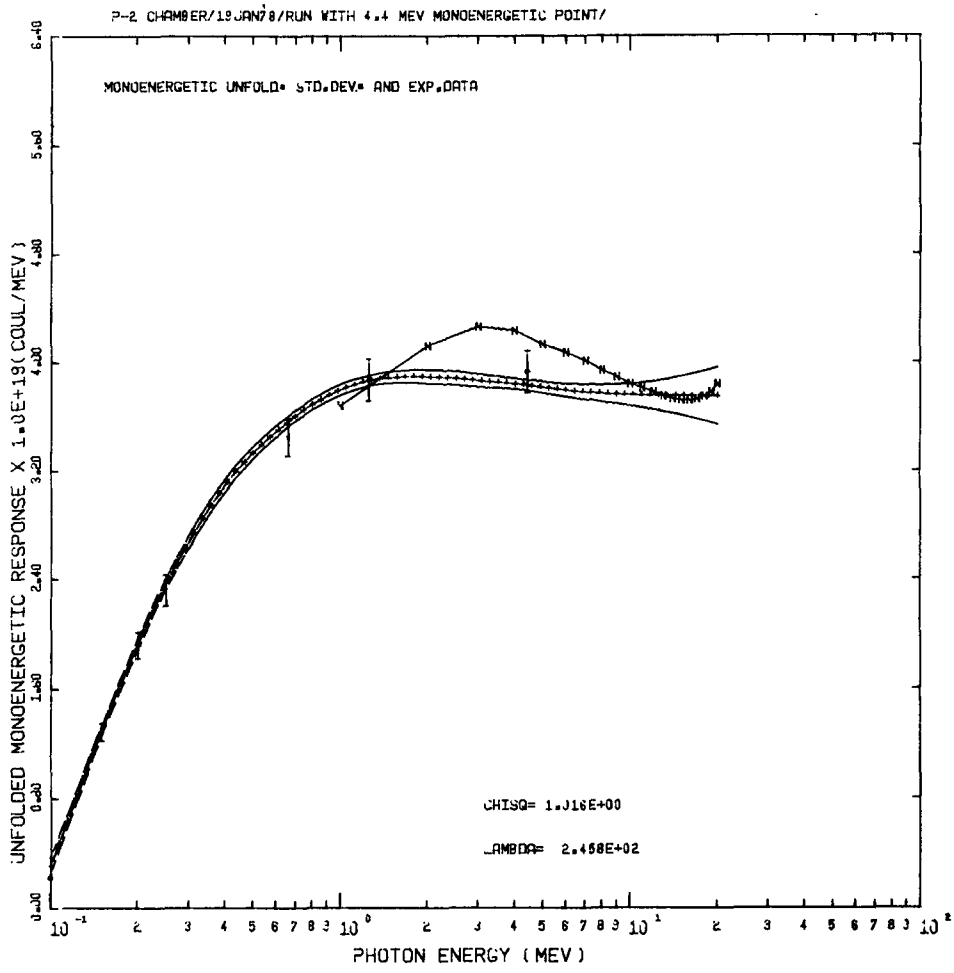

Fig. 17. Comparison of P-2 chamber derived sensitivities

The monoenergetic measurement shown as an asterisk and error bars at 4.4 MeV was generated by producing 4.4-MeV gamma radiation through the inelastic scatter of protons from ^{12}C at the LASL Van de Graaff accelerator facility. The gamma fluence was determined relative to a calibrated NaI spectrometer. The resulting P-2 chamber monoenergetic response at this energy was included in the analysis in the same manner as were the monoenergetic measurements of Pruitt and Domen.

Table 1 presents a tabulation of our determination of the P-2 chamber's monoenergetic sensitivity with standard deviation as a function of energy. The energy is expressed in MeV, and the sensitivity is expressed in units of coulombs of charge produced by the detector per MeV of gamma energy incident upon the detector. These values may be converted to commonly used units of coulomb/joule by division by a factor of 1.602×10^{-13} joule/MeV.

Table 1. P-2 chamber monoenergetic sensitivity versus energy

Photon Energy (MeV)	Detector Response Coul/(Gamma/MeV)	Standard Deviation Coul/(Gamma/MeV)	Photon Energy (MeV)	Detector Response Coul/(Gamma/MeV)	Standard Deviation Coul/(Gamma/MeV)	Photon Energy (MeV)	Detector Response Coul/(Gamma/MeV)	Standard Deviation Coul/(Gamma/MeV)
0.100	3.167E-20	5.072E-21	0.612	3.451E-19	3.775E-21	3.740	3.758E-19	5.058E-21
0.107	4.792E-20	4.541E-21	0.654	3.505E-19	3.668E-21	3.999	3.750E-19	5.046E-21
0.114	6.412E-20	4.140E-21	0.699	3.557E-19	3.615E-21	4.277	3.742E-19	5.024E-21
0.122	8.020E-20	3.844E-21	0.748	3.605E-19	3.597E-21	4.573	3.736E-19	4.995E-21
0.131	9.612E-20	3.628E-21	0.800	3.649E-19	3.594E-21	4.891	3.732E-19	4.963E-21
0.140	1.118E-19	3.472E-21	0.855	3.690E-19	3.589E-21	5.230	3.730E-19	4.933E-21
0.150	1.272E-19	3.368E-21	0.915	3.726E-19	3.572E-21	5.593	3.730E-19	4.911E-21
0.160	1.423E-19	3.311E-21	0.978	3.759E-19	3.540E-21	5.981	3.731E-19	4.908E-21
0.171	1.570E-19	3.286E-21	1.046	3.787E-19	3.495E-21	6.395	3.734E-19	4.935E-21
0.183	1.712E-19	3.287E-21	1.118	3.812E-19	3.451E-21	6.839	3.738E-19	5.006E-21
0.196	1.850E-19	3.314E-21	1.196	3.832E-19	3.426E-21	7.314	3.743E-19	5.140E-21
0.209	1.983E-19	3.376E-21	1.279	3.848E-19	3.443E-21	7.821	3.750E-19	5.351E-21
0.224	2.110E-19	3.464E-21	1.368	3.859E-19	3.526E-21	8.363	3.758E-19	5.654E-21
0.239	2.233E-19	3.575E-21	1.462	3.867E-19	3.657E-21	8.943	3.767E-19	6.060E-21
0.256	2.351E-19	3.701E-21	1.564	3.871E-19	3.819E-21	9.564	3.776E-19	6.577E-21
0.273	2.464E-19	3.869E-21	1.672	3.872E-19	3.996E-21	10.227	3.787E-19	7.206E-21
0.292	2.573E-19	4.033E-21	1.788	3.870E-19	4.173E-21	10.937	3.797E-19	7.945E-21
0.313	2.676E-19	4.186E-21	1.912	3.865E-19	4.342E-21	11.695	3.809E-19	8.792E-21
0.334	2.774E-19	4.312E-21	2.045	3.853E-19	4.496E-21	12.507	3.820E-19	9.740E-21
0.358	2.868E-19	4.403E-21	2.187	3.850E-19	4.632E-21	13.374	3.832E-19	1.079E-20
0.382	2.957E-19	4.451E-21	2.339	3.839E-19	4.748E-21	14.302	3.844E-19	1.192E-20
0.409	3.041E-19	4.454E-21	2.501	3.828E-19	4.844E-21	15.294	3.856E-19	1.314E-20
0.437	3.120E-19	4.411E-21	2.674	3.816E-19	4.921E-21	16.355	3.868E-19	1.444E-20
0.468	3.194E-19	4.327E-21	2.860	3.804E-19	4.980E-21	17.489	3.880E-19	1.581E-20
0.500	3.265E-19	4.208E-21	3.058	3.791E-19	5.021E-21	18.703	3.892E-19	1.725E-20
0.535	3.331E-19	4.066E-21	3.270	3.780E-19	5.047E-21	20.000	3.904E-19	1.875E-20
0.572	3.393E-19	3.915E-21	3.497	3.768E-19	5.059E-21			

The radiation dosimetry was standarized for future detector calibrations at LASL, LLL, and General Technical Services (GTS) at EG&G LVO through the P-2 chamber. LVO fabricated four P-2 ionization chambers from the NBS drawings to be used at the various radiation facilities. These chambers were compared with the Santa Barbara P-2 chamber and a similar detector on loan from Iowa State University utilizing a nominal 200-Ci ^{60}Co source and the linac with the standard bremsstrahlung target at energies of 6, 13, and 20.1 MeV using 1% momentum analyzing slit settings. At least six measurements were made at each energy with positive and negative bias on the chambers. Sensitivity ratios of the chambers are presented in Table 2. The response of ^{60}Co is the net current ratio of the particular chamber to that of the Santa Barbara P-2 chamber with a common collimation geometry. The bremsstrahlung measurements represent the

Table 2. P-2 chamber sensitivity ratios

Serial Number	^{60}Co	Bremsstrahlung End Point Energy (MeV)			Average Ratio
		6.0	13.0	20.1	
P2-SBO	1*	1*	1*	1*	1*
P2-001-LVO	0.990	0.980	0.988	0.983	0.985
P2-002-LVO	0.991	0.998	0.981	0.986	0.989
P2-003-LVO	0.986	0.967	0.978	0.991	0.980
P2-004-LVO	0.993	0.999	0.995	0.995	0.996
P2-I.S.U.	0.992	1.002	1.008	0.995	0.999

*Normalization standard

net current ratios of the particular chamber to that of the Santa Barbara P-2 chamber normalized to the bremsstrahlung target current. The standard deviation, σ, for the measurements is given by:

$$\sigma = \sqrt{\frac{n \sum_{i=1}^{n} X_i^2 - \left(\sum_{i=1}^{n} X_i\right)^2}{n(n-1)}} \qquad (19)$$

where

n = number of measurements performed

X_i = value of the i-th measurement

We note that the four newer (GTS) chambers are slightly lower in sensitivity than the Santa Barbara unit by 0.4 to 2%. However, the standard deviations show that the measurements are consistent. Comparison of our summary with Table 7 in the Pruitt and Domen monograph[1] shows a similar variation in other P-2 chambers. Of eleven chambers compared by NBS, an average difference factor of 1.0006 was reported with a standard deviation of 0.0103. The six units compared here have an average difference factor of 0.992 and a standard deviation of 0.009. These results should prove acceptable for the anticipated calibrations.

To determine if the P-2 chamber was subject to dose-rate saturation, beam parameters such as current, pulse width, repetition rate, and electron energy were varied over wide ranges. No saturation was observed at any combination of accelerator parameters. However, the P-2 chamber response was found to vary with position when used a straight wall collimator. This was attributed to wall scattering from the collimator and was eliminated by using multiple or tapered collimators. With a tapered collimator no variation in total radiation beam power as a function of distance was observed for distances from a few centimeters to two meters behind the tapered collimator.[23] Temperature and pressure corrections were made to the P-2 chamber measurements in the manner described by Pruitt and Domen.

This page left blank intentionally.

6. CONCLUSIONS

An experimental and analytical technique for obtaining detector monoenergetic sensitivities from a set of bremsstrahlung response measurements has been developed and applied to a number of useful radiation detectors including the P-2 standard ionization chamber. The sensitivities obtained in this manner are subject to experimental accuracy and to the inherently underdetermined nature of the problem. However, it has been shown that a physically plausible constraint can be applied in a statistically objective manner to obtain a reasonable solution which is consistent with direct measurement of the sensitivity made with isotopic sources. The resulting solution is directly a function of the experimental measurements and of the associated experimental errors.

Effects of the spot size of the electron beam incident upon the thick target are believed to be negligible, as are minor variations in beam position across the surface of the bremsstrahlung target. However, divergence of the electron beam appears to strongly effect the resulting bremsstrahlung spectrum, especially at the higher electron energies. Uncertainties in the total number of energetic electrons incident upon the target are due to penetration of the electrons through the target at higher energies (above 14 MeV), backscattering of the incident electrons from the target which becomes more significant below 5 MeV, and secondary electrons of low energy which may either escape from the target or drift down the beam line and perturb the target charge measurements.

The solution could be improved by 1) better knowledge of the actual bremsstrahlung spectrum incident upon the detectors, especially for lower electron energies, 2) improved accuracy of the experimental measurements, 3) performance of the measurements at both higher and lower energies, and 4) by use of a totally stopping calorimeter as an absolute radiation measurement standard.

Experiments are now underway to measure the bremsstrahlung spectrum more accurately. It is anticipated that an empirical correction or form factor can be applied to the Detch-Emigh bremsstrahlung calculation, to allow convenient and more accurate calculations of the bremsstrahlung from the standard target.

Remeasurement of the target charge correction factor to more accurately determine the ratio of charge collected on the target to the charge incident upon the detector could be expected to improve the accuracy of the data. Additional monoenergetic or isotopic response data in the vicinity of 2 to 3 MeV would be of considerable value in determining the shape of the P-2 chamber sensitivity in this region. Improved knowledge of this chamber's sensitivity, combined with verified knowledge of the bremsstrahlung spectrum produced by the standard thick target, would permit improved knowledge of this detector as a reference standard. Pruitt and Domen of NBS measured the response of the P-2 chamber to thin target bremsstrahlung for energies greater than 6.0 MeV, in reference to standard calorimeters. Response of the P-2 chamber to thick target bremsstrahlung could be obtained with greater accuracy by reference to a standardized calorimeter, or by improved knowledge of its monoenergetic sensitivity combined with improved knowledge of the actual thick target bremsstrahlung spectrum.

REFERENCES

1. J.S. Pruitt and S.R. Domen, "Determination of Total X-Ray Beam Energy with a Calibrated Ionization Chamber," NBS Monograph 48 (June 1962).

2. L.I. Schiff, *Phys. Rev., 83, 2,* 252 (1951).

3. J. Lewis Detch, Jr. and James L. Pigg, "Response Functions of Weapons Test Detectors," (Official Use Only), Report No. EGG 1183-2365, Santa Barbara Operations Number S-656-R (September 1977).

4. W.C. Anderson and L.P. Hocker, "Measured and Calibrated Energy Sensitivity of the LASL Compton Detectors," Report No. EGG 1183-2237, Santa Barbara Operations No. S-486-R (June 1970).

5. R. Knowlen, C. Sandifer, and J. Pigg, EG&G Santa Barbara Operations Memo No. APD-70-1023 (October 1970).

6. J. Mack, private communication.

7. T. Tabata, R. Ito, and S. Okabe, "An Empirical Equation for the Backscattering Coefficient of Electrons," *Nucl. Instrum. Methods, 94,* 509-513 (1971).

8. H. Bethe and W. Heitler, *Proc. R. Soc. A, 146,* 83 (1934).

9. H.W. Koch and J.W. Motz, *Rev. Mod. Phys., 31, 4,* 920 (1959).

10. M.J. Berger, *Methods in Computational Physics, Vol. 1,* 135, Academic Press (1963).

11. W.C. Dickinson and E.M. Lent, "Calculation of Forward Bremsstrahlung Spectra from Thick Targets," UCRL-50442 (6 June 1968).

12. E. Hisdal, "Bremsstrahlung Spectra Corrected for Multiple Scattering in the Target," *Phys. Rev., 105,* 1821 (1957).

13. C.R. Emigh, "Thick Target Bremsstrahlung Theory," LA-4097-MS (December 1969).

14. J.L. Detch, "Analytical Calculation of Multiple Component Thick Target Bremsstrahlung," to be published. (The work is an extension of the technique presented by C.R. Emigh, "Thick Target Bremsstrahlung Theory," LA-4097-MS, December 1969).

15. A.A. O'Dell, et al, "Measurement of Absolute Thick-Target Bremsstrahlung Spectra," EG&G Report No. EGG 1183-2139 (19 May 1967).

16. R.D. Evans, *The Atomic Nucleus,* McGraw-Hill Book Company, New York, 335 (1955).

17. U. Fano. H.W. Koch, and J.W. Mtoz, "Evaluation of Bremsstrahlung Cross-Sections at the High-Frequency Limit," *Phys. Rev., 112, 5,* 1679 (1958).

18. E.E. Osborne, "Smallest Least Squares Solutions of Linear Equations," *J. Siam Num. Ana., Ser. B, Vol. 2, No. 2,* 300-307 (1965).

19. P.J. Davis, "Orthonormalizing Codes in Numerical Analysis," *Survey of Numerical Analysis,* J. Todd, editor, McGraw-Hill, New York, 347-379 (1962).

20. J.R. Rice, "Experiments on Gram-Schmidt Orthogonalization," *Math. of Comput., 20,* 325-328 (1966).

21. Takio Tomimasu, "Absolute Measurements of High Energy X-Ray Beam Energy and Photoneutron Cross Sections for Natural Copper and Lead," Researches of the Electrotechnical Laboratory, Report No. 679, Electrotechnical Laboratory, Agency of Industrial Science and Technology, 2-Chome, Nagata-Cho, Chiyoda-Ku, Tokyo, Japan.

22. J.S. Pruitt and S.R. Domen, private communication.

23. C.W. Sandifer, "Measurements of Linac Bremsstrahlung Beam Intensity," Interoffice Memo No. SR&DD-012884, EG&G Santa Barbara Operations (13 June 1968).

DISTRIBUTION

DOE, NV

J.A. Koch
R.R. Loux
J. Newlin
R. Purcell

DOE, TIC, Oak Ridge

T.B. Abernathy (2)

LASL

S. Caldwell
D. Drake
J.G. Hopkins
P.B. Lyons
J. Mack
D.S. Metzger
C.S. Young

EG&G, Los Alamos Operations

W.C. Anderson
W. Broste

EG&G, Las Vegas Operations

P.A. Hawkins
J. Michaels
J.W. Trabert
P.H. Zavattaro

NBS, Gaithersburg

M. Berger
S.R. Domen
E. Hayward
J.E. Leiss
J.S. Pruitt

EG&G, Santa Barbara Operations

T. Davis
L. Detch (25)
L. Franks
L. Hocker
S. Lutz
M. Nelson
N. Norris
J. Pigg
P. Zagarino
Library
Publications (3)